






Combined *ab initio* and experimental screening of phase stabilities in the Ce-Fe-Ti-X system ($X = 3d$ and $4d$ metals)

Halil İbrahim Sözen ^{1,2} Semih Ener ³ Fernando Maccari ³ Bahar Fayyazi,³ Oliver Gutfleisch ³
Jörg Neugebauer,¹ and Tilmann Hickel ^{1,4}

¹Max Planck Institut für Eisenforschung GmbH, Max Planck Strasse 1, 40237 Düsseldorf, Germany

²Institute of Chemistry, Carl-von-Ossietzky University of Oldenburg, Oldenburg D-26129, Germany

³Functional Materials, Department of Material Science Technische Universität Darmstadt, 64287, Darmstadt, Germany

⁴BAM Federal Institute for Materials Research and Testing, 12489 Berlin, Germany



(Received 22 June 2022; revised 19 December 2022; accepted 9 January 2023; published 24 January 2023)

One of the main challenges for the synthesis and application of the promising hard-magnetic compound $\text{CeFe}_{11}\text{Ti}$ is the formation of Laves phases that are detrimental for their thermodynamic stability and magnetic properties. In this paper, we present an *ab initio* based approach to modify the stability of these phases in the Ce-Fe-Ti system by additions of $3d$ and $4d$ elements. We combine highly accurate free-energy calculations with an efficient screening technique to determine the critical annealing temperature for the formation of $\text{Ce}(\text{Fe},X)_{11}\text{Ti}$. The central findings are the dominant role of the formation enthalpy at $T = 0$ K on chemical trends and the major relevance of partial chemical decompositions. Based on these insights, promising transition metals to promote the stability of the hard-magnetic phase, such as Zn and Tc, were predicted. The comparison with suction casting and reactive crucible melting experiments for Ce-Fe-Ti-X ($X = \text{Cu}, \text{Ga}, \text{Co},$ and Cr) highlights the relevance of additional phases and quaternary elements.

DOI: [10.1103/PhysRevMaterials.7.014410](https://doi.org/10.1103/PhysRevMaterials.7.014410)

I. INTRODUCTION

Ab initio based methods are often combined with high-throughput screenings to design novel materials [1,2]. In these studies, the focus is usually on the optimization of the materials' properties at $T = 0$ K. The finite-temperature stability of the predicted compounds is, however, often a bottleneck for their synthesis, for the comparison with established experimental high-throughput screening methods, and eventually for applications. Thermodynamic databases for phase diagrams based on the CALPHAD method are usually not designed for novel material classes, whereas *ab initio* calculations of phase diagrams are usually limited to unary and binary systems. In the present paper, we therefore provide an *ab initio* based screening approach to improve the phase stability of multi-component compounds with respect to competing phases in the phase diagram by alloying.

The study is performed for permanent magnets, which are considered as key enablers for net-zero CO_2 emissions scenarios in the coming decades [3]. Here, materials design strategies are urgently needed since high-performance candidate materials such as Nd-Fe-B magnets [4,5] do strongly depend on chemical elements such as Nd, Dy, and Tb that are

rather critical and limited in availability [6,7]. This has stimulated efforts, both theoretically [8–10] and experimentally [11,12], to design new and alternative rare-earth (RE)-lean or RE-free hard magnetic materials, which will not be affected by the global supply monopoly and limited resources of RE elements.

One of the alternative elements that can replace critical REs like Nd, Dy, and Tb is the inexpensive [13] and abundant [14] element Ce. Similar to Nd- and Sm-based counterparts, Ce-based systems also form ThMn_{12} -type structures. The Nd- and Sm-based systems have similar intrinsic hard magnetic properties in comparison to the ternary benchmark $\text{Nd}_2\text{Fe}_{14}\text{B}$ systems [15–18]. However, the application of Ce in hard magnetic materials is connected with some challenges. The first challenge is the mixed valence state of Ce^{3+} and Ce^{4+} , which is the coexistence of trivalent $4f^1$ and tetravalent $4f^0$, being harmful for hard magnetic properties. As an example, the Ce valency was reported [19] to be 3.44 for $\text{Ce}_2\text{Fe}_{14}\text{B}$. Due to the mixed valence state of Ce, its compounds yield a lower magnetocrystalline anisotropy and Curie temperature compared to other RE-based magnets [20,21]. Nevertheless, the Ce valency is steric volume dependent [22,23], therefore, this feature can be beneficial to stabilize the Ce^{3+} configuration, which is desired for higher intrinsic magnetic properties via volume expansion. The Ce valency reduction by increasing volume suggests a substitutional doping. There are several experimental works that achieved the valency tailoring. For instance, the volume expansion is achieved by hydriding Ce-Fe-B-H alloys and it is seen that the Ce valency changed to Ce^{3+} [23,24].

Published by the American Physical Society under the terms of the Creative Commons Attribution 4.0 International license. Further distribution of this work must maintain attribution to the author(s) and the published article's title, journal citation, and DOI. Open access publication funded by the Max Planck Society.

The second challenge of Ce-based hard magnetic materials is the formation of the technologically less interesting CeFe₂ phase, which is actually highly detrimental for hard magnetic properties, in the microstructure [25,26]. It suppresses the crystallization of the desired hard magnetic CeFe₁₁Ti yielding a crucially reduced coercivity of these alloys and compounds [27–29]. The observations and effects of CeFe₂ were investigated previously [27,29–35] for corresponding Ce-based alloys. In our previous work, the formation of secondary CeFe₂ phase and its effect on the hard magnetic CeFe₁₁Ti phase stability was reported [36].

To overcome this challenge, we developed an *ab initio* based temperature-dependent screening approach for tailoring the phase stability of Ce-Fe-Ti-X (X = 3d and 4d elements) alloys. Cu is frequently used in RE-based permanent magnets to improve its magnetic properties [37–39]. Hence, we started with Cu substitution as a quaternary element and calculated the finite-temperature free energies. To further explore the applied methodology, we considered Ga as another substitution. Then, fundamental understanding achieved from these calculations is extrapolated to a large-scale screening to identify suitable elements X. This screening procedure provides a guideline for promising substitutional elements, which promote the formation of CeFe₁₁Ti and suppress the formation of secondary phases. Once we had the candidates for successful quaternary elements, we performed *ab initio* based finite-temperature free-energy calculations and compared our results with the ones obtained by the extrapolated screening. To our knowledge, there are no experimental efforts in the literature to stabilize ternary Ce-Fe-Ti hard magnetic phase by substitutional doping. Therefore, to be able to further compare the theoretical findings, we performed a high-throughput screening by using the reactive crucible melting (RCM) approach with theory-suggested elements. To complement the outcome of the RCM studies, a series of additional experiments were carried out by using the suction casting (SC) method. This method defers from the RCM as the solidification rates are faster, which gives the possibility to scan also the metastable states of the materials. Additionally, SC leads to a compositionally more restricted phase space as the overall composition of the samples are predefined nominally.

The paper is organized as follows. In Sec. II, we explain the technical aspects of our computational and experimental methods. In Sec. III, the effects of Cu and Ga substitutions are investigated based on *ab initio* calculations. In Sec. IV, the findings from Cu and Ga cases, implemented to the large-scale screening for 3d and 4d elements and promising quaternary elements are investigated. Furthermore, the verification of the screening approach is identified. In Sec. V, experimental findings are summarized with the comparison of theoretical work. We finally conclude the paper with remarks and discussions in Sec. VI.

II. COMPUTATIONAL AND EXPERIMENTAL DETAILS

A. Computational methodology

All first-principles calculations are based on density functional theory (DFT) as implemented in the Vienna *ab initio* simulation package VASP [40,41]. The ion-electron interac-

tions are treated by the projector-augmented wave (PAW) [42] method and the wave functions of valence electrons were expanded in a plane-wave basis set with a cutoff energy of up to 550 eV. In particular, the plane-wave basis was generated with the valence configuration of Ce-5s²5p⁶4f¹5d¹6s², where the single *f*-electron is treated explicitly as a valence state. The exchange-correlation is treated within the generalized gradient approximation (GGA) of Perdew-Burke-Ernzerhof (PBE) [43]. The treatment of correlated *f*-electrons in DFT is not straightforward and requires a Hubbard *U* correction. However, Ce-Fe compounds show a different behavior due to the hybridization of Ce-4*f* with Fe-3*d* electrons. Test calculations for the density states of CeFe₂ and the magnetic moments of CeCo₅ with *U* values up to 5 eV resulted into insignificant changes of the results. Therefore, in our calculations no Hubbard *U* correction scheme is applied (for more detailed discussions we refer Sec. 1.1 and Figs. S1-3 in the Supplemental Material [44]).

To calculate the phase stabilities of Ce-Fe-Ti-X alloys, DFT is not only applied to ground-state energies, but also to finite-temperature excitations [45]. We applied finite-temperature DFT calculations for the Ce-Fe-Ti ternary and for systems with Cu and Ga additions. For this purpose, Helmholtz free energies are considered as a function of crystal volume *V* and temperature *T* within the adiabatic approximation [46], therewith decoupling the degrees of freedom

$$F(T, V) = E_0(V) + F^{\text{el}}(T, V) + F^{\text{vib}}(T, V) + F^{\text{mag}}(T, V), \quad (1)$$

which treats the zero-temperature total energy E_0 , electronic F^{el} , vibrational F^{vib} , and magnetic F^{mag} contributions of the free energy.

The electronic contribution to the free energy F^{el} has its physical origin of the thermodynamic excitations of electrons close to the Fermi energy and was calculated employing the finite-temperature formulation of DFT by Mermin [47]

$$F^{\text{el}}(T, V) = E^{\text{tot}}(T, V) - E_0(V) - TS^{\text{el}}, \quad (2)$$

where E^{tot} is the total electronic free energy (including the binding energies at 0 K). We used the Monkhorst-Pack [48] scheme to sample the Brillouin zone. A dense mesh of *k*-points (kp) corresponding to $\sim 32 \times 10^3$ kp · atom satisfies the F^{el} below 1 meV/atom for considered alloys. S^{el} is the electronic entropy obtained from Fermi occupation numbers f_i

$$S^{\text{el}} = 2k_B \sum_i [f_i \ln f_i + (1 - f_i) \ln(1 - f_i)], \quad (3)$$

with k_B the Boltzmann constant.

The physical origins of the vibrational contribution F^{vib} are the phonons and they are computed with the *direct force constant method* [49,50]. This approach is based on the calculation of the Hellmann-Feynman forces for supercells containing several small atomic displacements (such as ~ 0.02 Å) according to the symmetry and number of different atom types. The convergence criteria to stop the electronic loop is also set to be 10^{-7} eV for all considered alloys. The eigenvalues of the Fourier transformed dynamical matrix ω_i enter the free-energy expression in harmonic approximation

[46]

$$F^{\text{vib}} = \frac{1}{N} \sum_i^{3N} \left\{ \hbar\omega_i + k_B T \ln \left[1 - \exp \left(-\frac{\hbar\omega_i}{k_B T} \right) \right] \right\}, \quad (4)$$

where \hbar is the reduced Planck constant. The summation in Eq. (4) runs over all $3N$ phonon states, where N is the number of atoms in the unit cell. In the *quasiharmonic approximation* considered here, the volume dependence of the phonon frequencies ω_i is additionally taken into account. Explicit anharmonic contributions are not considered.

The magnetic part of the total free energy F^{mag} is treated with an empirical formula proposed by Inden [51,52]. In this formulation, the mathematical expression for the magnetic heat capacity C_{mag} is similar for temperatures below and above

$$g(\tau) = \begin{cases} 0 & \tau \leq 0, \\ 1 - \frac{1}{D} \left[0.38438376 \frac{\tau^{-1}}{f} + 0.63570895 \left(\frac{1}{f} - 1 \right) \left(\frac{\tau^3}{6} + \frac{\tau^9}{135} + \frac{\tau^{15}}{600} + \frac{\tau^{21}}{1617} \right) \right] & 0 < \tau \leq 1, \\ -\frac{1}{D} \left(\frac{\tau^{-7}}{21} + \frac{\tau^{-21}}{630} + \frac{\tau^{-35}}{2975} + \frac{\tau^{-49}}{8232} \right) & \tau > 1, \end{cases} \quad (6)$$

$$D = 0.33471979 + 0.49649686 \left(\frac{1}{p} - 1 \right). \quad (7)$$

The optimized structural parameter p is 0.37 for bcc and 0.25 for non-bcc crystal structures. Since the notion of effective magnetic moments is most suitable for the material systems discussed in this work, we employ this approach. In this context, the magnetic entropy in the high-temperature limit $S_{\text{max}}^{\text{mag}}$ is written as

$$S_{\text{max}}^{\text{mag}} = k_B \sum_i x_i \ln(\beta_i + 1), \quad (8)$$

where x is the composition and β is the local magnetic moment. We used *ab initio* magnetic moments in the Inden model as an input.

However, the total magnetic free energy F^{mag} is the sum of ordered [as given in Eq. (5)] and disordered state contributions. The free-energy contribution from the paramagnetic disordering formally at infinitely high temperatures is considered by the expression

$$G_{\text{mag}}^{\text{PM}}(T) = RT \ln(\beta + 1), \quad (9)$$

where R is the gas constant. Further details of the model can be found in Ref. [54]. In addition to this, we investigated different recently proposed magnetic models based on Monte Carlo (MC) approaches. In a previous study [55], it was observed that the Inden model yields better agreement for heat capacity calculations of various alloys compared to experiments. More importantly, the MC models and the Inden model give consistent competition energies as defined in Eq. (10). No matter which method is chosen, a stabilization of the $\text{CeFe}_{11}\text{Ti}$ phase is only obtained at reasonable temperatures if the magnetic entropy contribution is taken into account [55].

T_C , despite the different physical origin for the magnetic entropy. This formula works with three input parameters, which are Curie temperature, the mean magnetic moment, and the magnetic enthalpy ratio of short- to long-range order. Chen and Sundman [53] modified the heat capacity expression to handle the phase transformation between the bcc and fcc phases of pure Fe. Xiong *et al.* [54] made another refinement to consider an effective magnetic moment rather than the mean magnetic moment to be able to take antiferromagnetic interactions into account. According to this work, the magnetic free energy in an ordered state as a function of relative temperature $\tau = T/T_C$ is given as

$$G_{\text{mag}} = T S^{\text{mag}} g(\tau), \quad (5)$$

B. Experimental details

To confirm the theoretical predictions, we carried out studies to screen the phase diagrams experimentally. For a broader screening of the phase diagram two different experimental approaches were used: (i) suction casting (SC) and (ii) reactive crucible melting (RCM). The SC method is a rapid solidification method which allows stabilization of possible metastable structures due to rapid cooling. In addition, as a result of rapid solidification, the obtained microstructure is composed of small grains (size below 10 μm) as reported elsewhere [17]. Another feature of the SC is the limitation of the compositional space as the starting composition is well defined. Further, the RCM method is a high-throughput screening method where the obtained phases are generally limited to the equilibrium conditions. The RCM method was already applied to a broad range of material systems [56–58].

The SC experiments were carried out by using an arc-melting-setup-equipped actively cooled plate cavity to form bulk rectangular ingots of 0.5-mm thickness. During the SC process, the material is made molten by an electrical arc and the material in the molten state is sucked to a cavity with chamber over pressure. Prior to the casting the alloys were prepared by using an induction melter. For the investigation, as suggested by the theoretical predictions, the $\text{Ce}_{14}\text{Fe}_{70}\text{Ti}_{13}\text{X}_3$ composition is selected for $\text{X} = \text{Cu}, \text{Ga}, \text{Co},$ and Cr . As a reference a $\text{Ce}_{14}\text{Fe}_{72}\text{Ti}_{14}\text{X}$ sample was also prepared. After suction casting, the resulting plates were annealed at 1000 $^\circ\text{C}$ (1273 K) for 12 hours to ensure homogeneity.

The RCM experiments were carried out in iron crucibles filled with the powders of Ce, Ti elemental powder. For the observation of the effect of the X element on the phase stability different crucibles were prepared with additional el-

emental powders of $X = \text{Cu, Ga, Co, and Cr}$. Powder-filled crucibles were sealed under Ar atmosphere, then sealed in a quartz tube and annealed for 96 hours at 850 °C (1123 K) and 1000 °C (1273 K) to ensure proper diffusion and equilibrium condition. The crucibles were quenched into water, cut into halves, and polished for characterization. Phase distribution analysis and chemical compositional determination were done by using a TESCAN scanning electron microscopy (SEM) in backscattered electron (BSE) contrast mode using energy dispersive x-ray (EDX) analysis. To obtain a good statistical distribution and reduce the error, the measurements were carried out at multiple points and at different locations of the crucibles.

III. IMPACT OF THE SUBSTITUTIONS $X = \{\text{Cu, Ga}\}$ IN Ce-Fe-Ti-X

To computationally predict the critical temperature for the thermodynamic stability of the hard magnetic $\text{CeFe}_{11}\text{Ti}$ phase, we determine the competition energy

$$\begin{aligned} F^{\text{comp}} &= (F[\text{CeFe}_2] + F[\text{Fe}_2\text{Ti}] + 7F[\text{Fe}]) - F[\text{CeFe}_{11}\text{Ti}] \\ &= F^{\text{dec}} - F[\text{CeFe}_{11}\text{Ti}]. \end{aligned} \quad (10)$$

It considers the free-energy differences between the desired hard magnetic phase and the three competing phases CeFe_2 , Fe_2Ti , and Fe . Opposite to our previous work [36], the phase $\text{CeFe}_{11}\text{Ti}$ is taken as a reference. It is stable if F^{comp} is positive, while a negative energy value indicates that the decomposition (decomp) is energetically favorable and in particular the Laves phase CeFe_2 will form.

The lower part of Fig. 1 illustrates the finite-temperature dependence of the competition energy for the Ce-Fe-Ti ternary to compare it with the impact of Cu and Ga substitutions. It can be seen that, in the ternary case, without substitutional element (labeled “Full decomp wo subs.”), there is a driving force on $\text{CeFe}_{11}\text{Ti}$ (which will be referred to as 1:12) for decomposition of 174 meV/f.u. at 0 K. Therefore, the 1:12 phase is unstable below 710 K, as compared to the formation of the considered competing phases. This observation is decisive for the design and sustainability of the promising hard magnetic phase $\text{CeFe}_{11}\text{Ti}$.

The inclusion of quaternary alloying elements, such as Cu and Ga , yields a modification of the different free-energy terms in the competition energy in Eq. (10). Since the concentrations of the solutes c_X^{SC} in the employed supercells do not match the concentrations in the real materials, linear combinations such as

$$\begin{aligned} F[\text{CeFe}_2] &\rightarrow F[\text{CeFe}_2] \left(1 - \frac{c_X^{\text{CeFe}_2}}{c_X^{\text{SC}}}\right) \\ &+ \frac{1}{8} F[\text{Ce}_8\text{Fe}_{15}\text{X}] \frac{c_X^{\text{CeFe}_2}}{c_X^{\text{SC}}} \end{aligned} \quad (11)$$

are considered.

The actual concentrations of the solute will not be the same in the different intermetallic phases and, therefore, need to be determined in several steps. First, the solution enthalpy E^{sol} at 0 K is determined for all the sublattices of the individual phases to analyze their occupation. In the case of the Fe

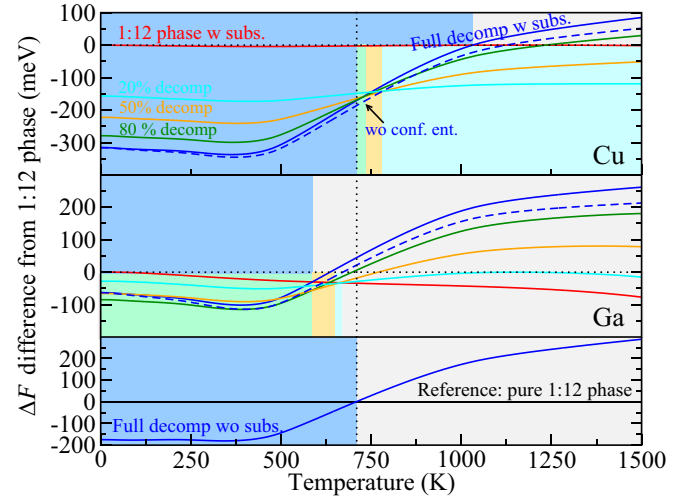


FIG. 1. Calculated finite-temperature competition energy without the alloying element (lower part) and with substitutions of 3 at. % Ga and Cu . The zero energy reference is, in all cases, the free energy of the 1:12 phase without substitution. Different volume fractions η of the decomposed phases (designated with cyan: 20 decomp.; orange: 50% decomp.; and green: 80% decomp.) are considered where 100% corresponds to a full decomposition blue line. The color coding indicates the stability regions for such a partial (full) decomposition below (above) the zero line, respectively. The dashed line indicates the change of the result if configurational entropy were not considered. Note the different sign convention as compared to Ref. [36].

sublattices, the corresponding expressions are

$$\begin{aligned} E_{\text{CeFe}_{11}\text{Ti}}^{\text{sol}} &= E[\text{Ce}_2\text{Fe}_{21}\text{Ti}_2\text{X}] - \mu_X + \mu_{\text{Fe}} - E[\text{Ce}_2\text{Fe}_{22}\text{Ti}_2], \\ E_{\text{CeFe}_2}^{\text{sol}} &= E[\text{Ce}_8\text{Fe}_{15}\text{X}] - \mu_X + \mu_{\text{Fe}} - E[\text{Ce}_8\text{Fe}_{16}], \\ E_{\text{Fe}_2\text{Ti}}^{\text{sol}} &= E[\text{Fe}_7\text{Ti}_4\text{X}] - \mu_X + \mu_{\text{Fe}} - E[\text{Fe}_8\text{Ti}_4], \\ E_{\text{Fe}}^{\text{sol}} &= E[\text{Fe}_{53}\text{X}] - \mu_X + \mu_{\text{Fe}} - E[\text{Fe}_{54}]. \end{aligned} \quad (12)$$

Here, the subindices in the squared brackets correspond to the atoms per supercell used in the DFT calculations. In each phase, a single solute atom X is added, which gives rise to the following supercell concentrations c_X^{SC} : 3.8 at.% for $\text{CeFe}_{11}\text{Ti}$, 4.2 at.% for CeFe_2 , 8.3 at.% for Fe_2Ti , and 1.8 at.% for Fe_{54} .

At this step the exchange of atoms is described with respect to a chemical reservoir μ_X [59] that is determined by the ground-state energies of the substituted elements. μ_{Fe} is the chemical potential for ferromagnetic bcc Fe. We conclude from this analysis that Cu and Ga (as well as for the majority of the solute atoms studied below) prefer the Fe sublattices. Therefore, we restrict the following considerations to substitutions of Fe atoms only, i.e., the solute X does not replace a Ce and Ti atom in any of the phases in F^{comp} . In addition, the substitution of the solute X in grain boundaries, surface oxides, or other microstructure features is excluded, while the potential formation of new phases is briefly discussed in a separate section. The complexity connected with the stability analysis of the quaternary system makes these simplifications necessary.

A. Chemical potential for full decomposition

Once we identified the preferential Fe sublattice sites for the quaternary alloying elements, the finite-temperature formation free energy is calculated in each considered phase. For example,

$$\Delta F_{\text{CeFe}_2}^{\text{form}} = F[\text{Ce}_8\text{Fe}_{15}\text{X}] - F[\text{Ce}_8\text{Fe}_{16}] - \Delta\mu. \quad (13)$$

This provides access to the substitutional concentrations [60] in the different phases

$$c_{\text{X}}^{\text{Fe}}(\Delta\mu) = f_{\text{Fe}} \exp\left(\frac{-\Delta F_{\text{Fe}}^{\text{form}}}{k_{\text{B}}T}\right), \quad (14)$$

$$c_{\text{X}}^{\text{CeFe}_2}(\Delta\mu) = f_{\text{CeFe}_2} \exp\left(\frac{-\Delta F_{\text{CeFe}_2}^{\text{form}}}{k_{\text{B}}T}\right), \quad (15)$$

$$c_{\text{X}}^{\text{Fe}_2\text{Ti}}(\Delta\mu) = f_{\text{Fe}_2\text{Ti}} \exp\left(\frac{-\Delta F_{\text{Fe}_2\text{Ti}}^{\text{form}}}{k_{\text{B}}T}\right), \quad (16)$$

where f_{σ} is the fraction of the atoms that belong to the relevant sublattice in phase σ , i.e., $f_{\text{Fe}} = 1$ and $f_{\text{CeFe}_2} = 2/3$ (16a sublattice). For Fe_2Ti the fraction is $f_{\text{Fe}_2\text{Ti}} = 1/2$ (6h sublattice), $1/6$ (2a sublattice), or $2/3$ (if the solution enthalpy for 6h and 2a is almost degenerate). The concentrations are determined at a fixed temperature close to the critical temperature for decomposition since the exchange of the solutes between the phases is kinetically suppressed at lower temperatures. Nevertheless, possible implications of a thermodynamic equilibration throughout a larger temperature interval are discussed in the Supplemental Material (see Fig. S4-S6).

In Eq. (13), the difference of the chemical potential of the solute X and the host atom Fe

$$\Delta\mu = \mu_{\text{X}} - \mu_{\text{Fe}}, \quad (17)$$

can now be chosen such that the total atomic concentration of the substitutional element distributed in the decomposed phases

$$c_{\text{X}}^{\text{dec}}(\Delta\mu) = \frac{3}{13}c_{\text{X}}^{\text{CeFe}_2}(\Delta\mu) + \frac{3}{13}c_{\text{X}}^{\text{Fe}_2\text{Ti}}(\Delta\mu) + \frac{7}{13}c_{\text{X}}^{\text{Fe}}(\Delta\mu) \quad (18)$$

is identical to the nominal concentration of the solute, i.e., 3 at.%. Here, an equal chemical potential throughout all three competing phases after the decomposition is assumed and the reservoir is no longer defined by the ground state of the pure elements. The prefactors in Eq. (18) are determined by Eq. (10). The same kind of canonical constrain determines also the chemical potential in the 1:12 phase

$$c_{\text{X}}^{\text{CeFe}_{11}\text{Ti}}(\Delta\mu^{(1:12)}) = 3 \text{ at.}\%. \quad (19)$$

The consequence of these concentrations on the free energies that form the competition energy in Eq. (10) can be seen in the upper parts of Fig. 1. Here the red lines (labeled “1:12 phase w subs.”) provide the impact of the solutes on the temperature dependence of $F[\text{Ce}_2\text{Fe}_{21}\text{Ti}_2\text{X}]$. Its value at $T = 0$ K is again taken as a reference. According to Eq. (10) this phase is in competition with the free energy $F^{\text{dec}}(c_{\text{X}}^{\text{dec}} = 3\%)$ of the other three phases, given by the blue solid lines (labeled “full decomp w subs.”). The shading above the zero lines highlights the respective stability regions.

The main message of Fig. 1 is a substantial shift of the intersection of the full decomposition free energies and the free energies of the 1:12 phase due to the impact of the solutes on the different phases. In the case of Cu substitution, the formation temperature of the 1:12 phase increases from 710 K to 1050 K. This is because it is energetically most favorable for Cu atoms to substitute the Fe atoms in the CeFe_2 phase, both due to the solubility at $T = 0$ K and due to the increased vibrational entropy of CeFe_2 (vibrational entropy of $\text{CeFe}_{11}\text{Ti}$ is hardly changed by Cu). The resulting stabilization of the CeFe_2 phase causes the decrease in the competition energy and the destabilization of the ternary phase.

In the case of Ga substitution, the critical formation temperature of the $\text{CeFe}_{11}\text{Ti}$ phase decreases to 610 K. This is due to the fact that Ga is stabilizing the 1:12 phase more than the competing phases. Therefore, Ga can be considered as a suitable candidate to improve the thermodynamic stability of the desired hard magnetic phase in the Ce-Fe-Ti system, whereas Cu seems to be detrimental.

We note that the chemical potentials should also carry a temperature dependence given by the configurational entropy related to the fraction of symmetrically equivalent sites of a given sublattice. We combine these contributions to an additional entropy contribution to the free energy of each phase σ

$$S_{\sigma}^{\text{conf}} = k_{\text{B}}f_{\sigma} \left[\frac{c_{\text{X}}^{\sigma}}{f_{\sigma}} \ln\left(\frac{c_{\text{X}}^{\sigma}}{f_{\sigma}}\right) + \left(1 - \frac{c_{\text{X}}^{\sigma}}{f_{\sigma}}\right) \ln\left(1 - \frac{c_{\text{X}}^{\sigma}}{f_{\sigma}}\right) \right], \quad (20)$$

where f_{σ} is again the sublattice fraction in this phase. To highlight the contribution of this term, the blue dashed line in Fig. 1 provides the free energies if there were no configurational entropy. It can be seen that this term does not change the trends qualitatively.

B. Chemical potential for partial decomposition

The full decomposition of the 1:12 phase discussed so far will yield a jump in the chemical potential at the phase transformation. This is because the two conditions (19) and (18), before and after the decomposition, respectively, usually give rise to different chemical potentials. In a more general approach, therefore, only a certain volume fraction η is assumed to decompose, while the remaining volume fraction $(1 - \eta)$ is still in the $\text{CeFe}_{11}\text{Ti}$ phase. In such a scenario, a chemical equilibrium between all four phases should be ensured such that

$$\eta c_{\text{X}}^{\text{dec}}(\Delta\mu) + (1 - \eta)c_{\text{X}}^{\text{CeFe}_{11}\text{Ti}}(\Delta\mu) = 3 \text{ at.}\%. \quad (21)$$

This represents the case that an increased concentration of the solute X changes the stability of the decomposed phases relative to the 1:12 phase, but the limited total amount of the solute (i.e., 3 at.% in our case) only allows such an increase for a certain volume fraction. In the case of Cu, for example, the solubility in the CeFe_2 phase is comparatively high. As a consequence, if only $\eta = 20\%$ of the $\text{CeFe}_{11}\text{Ti}$ phase were decomposed, then the expression (21) would yield a Cu concentration of 40 at.% in the CeFe_2 phase.

Since this is energetically highly favorable, the modified free energy

$$F^\eta = \eta F^{\text{dec}}(c_X^{\text{dec}}) + (1 - \eta)F[\text{CeFe}_{11}\text{Ti}, c_X^{\text{CeFe}_{11}\text{Ti}}] \quad (22)$$

is well below the free energy $F[\text{CeFe}_{11}\text{Ti}, 3\% \text{ Cu}]$, as can be seen in Fig. 1. In contrast to this, a full decomposition for the same total amount of Cu yields a Cu concentration of 13 at.% in the CeFe_2 phase and the volume fractions of the Fe phase and the Fe_2Ti phase gets a much larger weight when determining the free energy. Similarly to the Cu-free case, this suppresses the decomposition at high temperatures.

Using this methodology, we learn in the case of Cu addition that, even at high temperatures, the 1:12 phase is not fully stable. Instead a certain volume fraction of the Laves phase CeFe_2 will always form, which accommodates most of the Cu. On the other hand, a partial decomposition is also energetically more favorable than the full decomposition. Therefore, an increasingly large volume fraction of the 1:12 phase can also be observed at temperatures between 710 K and 1050 K, where this phase was predicted to be unstable in full decomposition. This fraction decreases when approaching the critical temperature for the solute-free case, but remains finite before a complete decomposition into Fe and the Laves phases is observed at about 710 K. Overall, the addition of Cu does not improve the stability of the 1:12 phase, but stabilizes a certain volume fraction of the CeFe_2 phase in temperature regions where otherwise the pure 1:12 phase could be expected.

The often-reported improvement of hard-magnetic properties by Cu [37–39] is, therefore, not connected to phase stabilities. Indeed, experiments indicate a segregation of Cu to intergranular regions (i.e., grain boundaries and triple junctions) of conventional Nd-Fe-B magnets and the formation of a nonmagnetic layer that improves the coercivity. It was also reported in another *ab initio* study [61] that Cu tends to avoid substituting atoms in the grain interiors of $\text{Nd}_2\text{Fe}_{14}\text{B}$.

The situation is opposite in the Ga case. Here the $T = 0$ K energies yield a strong preference for an incorporation of the solute in the 1:12 phase. There is also a noticeable increase of the entropy of the Laves phases, but this is partly compensated by the changes in the vibrational entropy of $\text{CeFe}_{11}\text{Ti}$. This yields the extended stability region of the pure 1:12 phase already described above. Still one observes also in this case a temperature regime in which a partial decomposition takes already place though the full decomposition is not yet favorable. Highly interesting is the fact that, even down to low temperatures, a small volume fraction (20%) of $\text{CeFe}_{11}\text{Ti}$ that accommodates almost all the Ga atoms benefits from the strongly increased Ga concentration (=13 at.% in this case) and becomes more stable than the competing phases. This volume fraction of the 1:12 phase cannot increase at low temperatures because the Ga content then becomes too dilute to ensure such a stabilization.

We note that the solute concentrations in partially decomposed phases can be well beyond the dilute limit (e.g., $\eta = 20\%$ yields 60 at.% Cu on the $6a$ sublattice), and therefore the linear interpolation (11) and, therewith, the predictive power of our approach can be questionable.

IV. SCREENING THE IMPACT OF SUBSTITUTIONS IN Ce-Fe-Ti-X

The examples of small additions of Cu and Ga have already demonstrated that chemical alloying has a considerable impact on the critical formation temperature of $\text{CeFe}_{11}\text{Ti}$. To improve the impact, we systematically investigate the effect on phase stabilities caused by an additional solute from the $3d$ and $4d$ transition metals. These alloying elements were already previously considered for improving hard magnetic materials by high-throughput screening calculations [8,9,62,63]. However, these efforts were limited to intrinsic magnetic properties and the thermodynamic stability of the suggested alloys was not considered.

To close this gap, thermodynamic calculations as introduced for Cu and Ga can be done, but are computationally too demanding to be performed for a large number of solutes. We, therefore, employ an efficient screening scheme instead that reduces the number of demanding calculations to a few selected cases. To this end, we benefit from our observation that the impact of the added solutes is to a large extent captured by the energetics at the ground state.

A. Focus on the energetics at $T = 0$ K

At $T = 0$ K, the driving force of decomposition according to Eq. (10) is for the ternary system without solutes 174 meV/f.u. This number is substantially (i.e., in the order of 100 meV/f.u.) changed by substituting only 3 at.% of the Fe atoms. It increases to 315 meV/f.u. if Cu is added, implying an (at least partial) decomposition of the 1:12 phase over a much larger temperature range than without Cu. In the case of Ga it decreases to 63 meV/f.u., resulting in temperature ranges that are only partially decomposed or completely free of Laves phases, while a full decomposition is expected without Ga.

These changes at $T = 0$ K need to be compared with the impact of the solutes on the free energies contributing to the competition energy in Eq. (10). To this end, we concentrate on the results for the full decomposition shown in Fig. 1 and note a strong similarity between the temperature dependence in the ternary Ce-Fe-Ti and the Cu and Ga containing cases. In Fig. 2 the competition energies F^{comp} for different compositions are aligned at $T = 0$ K. Comparing the free energies of alloys with Cu and Ga additions, the difference is negligible. The small concentration (3 at. %) of alloying elements apparently has a similar and small impact on the lattice vibrations and the magnetic moments. The qualitatively different impact of Cu and Ga on the phase stability is therefore clearly determined by the ground-state energetics.

A closer inspection reveals that the perfect agreement at finite temperatures for Cu and Ga additions is coincidence (see Fig. S4). The solutes have different impacts on the individual free-energy contributions of F^{comp} . The free energy of individual phases can, by some solutes, be changed by up to 80 meV/f.u. at 1500 K. However, the qualitative trend is in particular for the 1:12 phase and the CeFe_2 Laves similar, leading to compensation effects. One can conclude from Fig. 2 that the deviations caused by the solutes are below 50 meV/f.u. at 1000 K and below 20 meV/f.u. at 500 K.

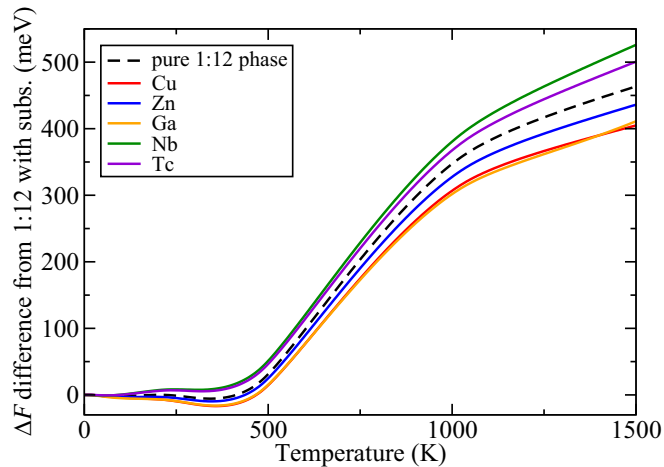


FIG. 2. Competition free energy F^{comp} as calculated by Eq. (10). The results for the ternary Ce-Fe-Ti case (black dashed line) and for different solute additions (colored solid lines) are aligned at $T = 0$ K. The impact of the solute species on the competition free energies is visible.

This is still substantially less than the changes in the formation enthalpies at $T = 0$ K.

The working assumption for the following screening of various transition metals is, therefore, that the qualitative impact of these solutes on the phase stability of $\text{CeFe}_{11-y}\text{Ti}_x$ is determined by the energetics at $T = 0$ K. As a consequence, the computationally less expensive ground-state energies can be used for selecting potential candidates that improve this stability.

We note, however, that finite-temperature entropy contributions enter the thermodynamics not only in the free energy terms in Eq. (10), but they also modify the free energies of formation that determine the distribution of elements among the differences in chemical equilibrium, as described by Eqs. (14) to (16). Also in this case the impact of the alloying elements is largely described by the energetics at $T = 0$ K (see Fig. S7).

The explicit temperature in the Boltzmann coefficients in Eqs. (14) to (16) can, of course, not be set to zero since this would suppress a distribution of the alloying elements among the different phases. Here we stick to the assumption that a temperature close to the onset of the formation of the Laves phases should be chosen since solute redistribution at lower temperatures is kinetically suppressed. According to our analysis, the actual choice of this temperature (700 K and 1200 K are compared in Fig. S4) is of secondary importance.

B. Sublattice preference at 0 K

The first set of calculations in our screening scheme is devoted to the solution enthalpies according to Eq. (12), including the possible substitution of Ti and Ce sites. The *ab initio* data for the ground states of the considered substitutional elements, which determine μ_X , are given in the Supplemental Material Table S2 (see also Refs. [64–79]).

The energetic preference for the substitution of atoms at the different Wyckoff positions can be obtained from Fig. 3. $\text{CeFe}_{11}\text{Ti}$ consists of four sublattices, but we distinguish between the substitution of an Fe atom and a Ti atom at the

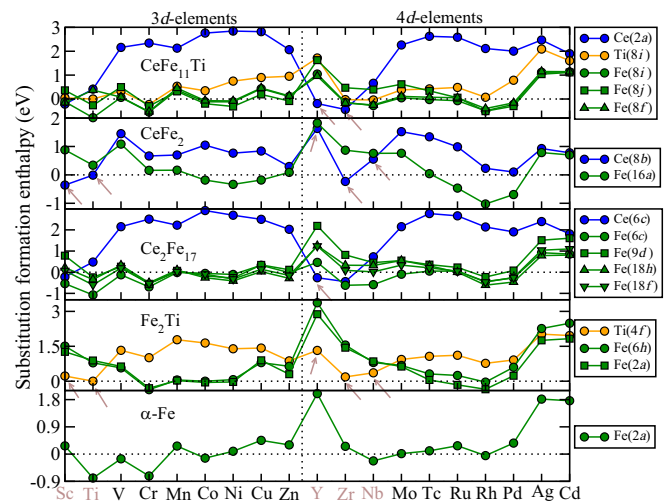


FIG. 3. Formation enthalpies to substitute 3d and 4d elements at different Wyckoff positions in $\text{CeFe}_{11}\text{Ti}$, CeFe_2 , $\text{Ce}_2\text{Fe}_{17}$, Fe_2Ti , and Fe, respectively. In the majority of the cases Fe sublattices are preferred, but Sc, Ti, Y, Zr, and Nb are exceptions that yield, in some phases, lower energies for Ce and Ti sublattices (brown labels and arrows). In these cases, we still consider Fe sublattice formation energies only.

$\text{Fe}(8i)$ site. Although $\text{Ce}_2\text{Fe}_{17}$ is not considered as a competing phase in Eq. (10), we also determined the preferential sites for this phase to interpret the RCM experimental results and to extend the considerations on substitutional partitioning. In fact, both the rhombohedral 2:17 phase and the tetragonal 1:12 phase can be derived from the 1:5 structure by replacing different fractions of the RE atoms with pairs of TM elements (see Ref. [80] for details). We observe for all phases an energetically preferred substitution of the Fe sublattices, which fits to the consideration of the phase diagram in Eq. (10) and supports our approach in Eqs. (13) and (17) to focus on the Fe sublattice.

More precisely, in the case of $\text{CeFe}_{11}\text{Ti}$, substitutional elements with a 3d or 4d shell that is less than half filled, prefer to occupy the $\text{Fe}(8i)$ site, while for the more than half-filled elements the $\text{Fe}(8j)$ site is more favorable. In general, the substitution on the Ce site yields largely positive formation enthalpies, which excludes a substitution of this site by 3d and 4d elements. The only exceptions are Sc, Y, and Zr. Due to the structural similarities of the two phases, the formation enthalpies in $\text{Ce}_2\text{Fe}_{17}$ are in good agreement with those in $\text{CeFe}_{11}\text{Ti}$.

In the case of CeFe_2 less than half-filled 3d and 4d elements, which are Sc, Ti, Y, Zr, and Nb, tend to substitute the Ce site. For the Fe_2Ti case, both 6h and 2a Fe sublattices show similar formation enthalpies. Here, Sc, Y, Zr, and Nb are again exceptions preferring to occupy the Ti site. Since a Ce or Ti substitution would require to handle a more complex interplay of chemical potentials $\Delta\mu$ than that used in Eq. (17), we chose the energetically favorable Fe sites for those elements. In this way, a systematic trend study for the energetics for 3d and 4d elements is possible. For instance, Sc prefers to be substituted at a $\text{Ti}(4f)$ site in the Fe_2Ti phase, but we assume that Sc is placed in $\text{Fe}(2a)$.

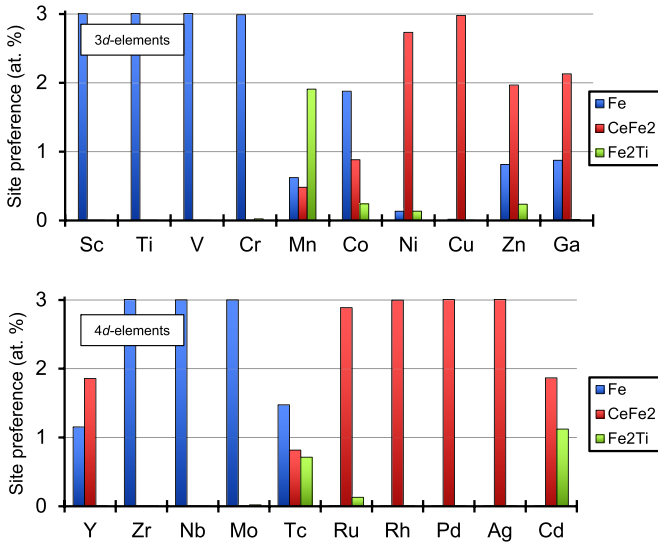


FIG. 4. Compositional distribution of the considered 3d and 4d elements among the competing phases, using the ground-state formation energies in Fig. 3 and assuming a Boltzmann statistics at 1200 K. The total concentration of substitutional elements that are distributed over the three phases is 3 at. % as a dilute limit, see Eq. (18). It is assumed that full decomposition takes place and that solutes substitute Fe atoms only.

C. Chemical equilibrium at 1200 K

After the preferred lattice sites of each phase are identified, the finite-temperature distribution of the alloying elements can be calculated according to Eqs. (14) to (16). To this end, the ground-state formation energies are used in the exponent and only the explicit temperature dependence $k_B T$ is considered at 1200 K. A detailed evaluation documented in the Supplemental Material (Fig. S4) justifies this approximation. The difference to a full treatment of the temperature dependence is negligible for Cu, while for Zn the relative solubility in the CeFe_2 phase decreases by 30% and for Ga it increases by 50%. Nevertheless, the critical temperature for full decomposition does not change by more than 50 K.

The results shown in Fig. 4 indicate that the 3d and 4d elements with less than half-filled d shells will mainly enter the pure Fe phase. Only Y enters CeFe_2 and Fe simultaneously. For the case of half-filled d -shells (i.e., both for Mn and Tc), we do not see a clear preference for a specific phase but a distribution over all three competing phases. In the case of elements with more than half-filled d shells, we see a strong preference of the CeFe_2 phase. The only exception is Co that prefers the substitution of Fe, which may be caused by magnetic interaction energies. While we consider the distribution of alloying elements over competing phases, in the case of the hard magnetic $\text{CeFe}_{11}\text{Ti}$ phase we always assume that all the alloying elements (3 at. %) are substituted at the energetically most favorable site.

D. Competition energies

Once the distribution of the considered solute elements among the competing phases is known, the competition energy is for each solute calculated at $T = 0$ K. As can be seen

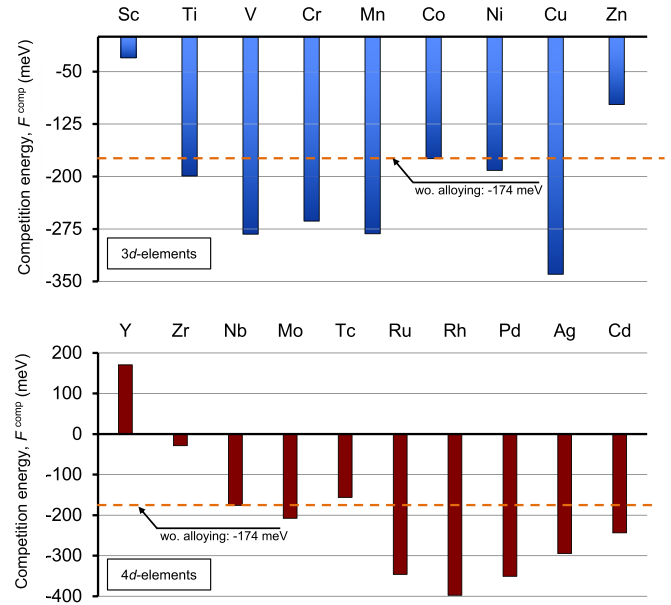


FIG. 5. Competition energies of phases alloyed with 3d and 4d elements at 0 K. The horizontal dashed lines show the competition energy in the case of the Ce-Fe-Ti ternary.

in Fig. 5, Cu shows among the 3d elements the strongest driving force for a decomposition. In this case, the competition energy at 0 K increases from 174 meV for the ternary alloy to 322 meV. The other elements with a more than half-filled 3d shell perform better than the 3d elements with less than half-filled shells. In particular, Zn shows a competition energy as low as 97 meV at 0 K, followed by Co and Ni. The low competition energy in the case of Sc substitution is artificial because Sc is one of the exceptional elements that does not prefer Fe sites and the underlying calculations for the binary phases are not considering the energetically most favorable site. Only if the chemical potentials of Ce and Ti were indeed such that Sc prefers the solution into pure Fe, a strong preference of the $\text{CeFe}_{11}\text{Ti}$ would be observed.

In the case of the 4d elements the situation is opposite to the 3d elements in the sense that substitutional elements with less than half-filled 4d shells yield a lower driving force for decomposition than those with more than half-filled shells. In the case of alloying with Tc, the competition energy is found to be 156 meV, which appears to be the best candidate among the 4d elements. The second candidate is Mo with a competition energy of 207 meV, which is already above the ternary case. The situation of Y, Zr, and Nb is similar to that of Sc as the substitution is not considered at the energetically most favorable Ti or Ce sites. The corresponding competition energies are artificially low, unless the Ti or Ce chemical potentials are indeed high enough to drive the alloying elements after decomposition into pure Fe.

Following the discussion in the context of Fig. 2, we can use the 0 K competition energies for all solutes and the entropy contributions of the ternary Ce-Fe-Ti system to estimate the critical temperature for full phase decomposition. As can be seen in Fig. 6(a), the formation temperature is reduced to 610 K in the case of Zn alloying and to 680 K in the case of Tc.

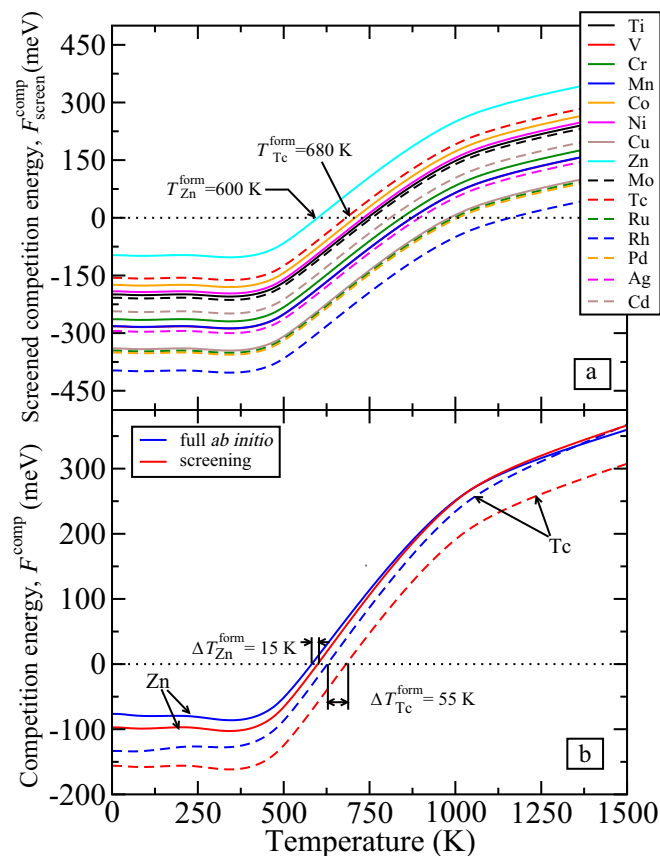


FIG. 6. (a) Competition energies of phases alloyed with 3d (solid lines) and 4 elements (dashed lines) at finite temperatures. Finite-temperature effects are added from the ternary Ce-Fe-Ti case and configurational entropies are included. (b) Comparison of the competition energies of the explicitly calculated finite-temperature entropy terms (blue lines) and the screening method based on 0 K enthalpies (red lines) for alloying with Zn (solid lines) and Tc (dashed lines). The difference in the critical formation temperature is highlighted by arrows.

While this screening of critical temperatures is based on the energetics at $T = 0$ K, a more accurate free-energy calculation for the most promising alloying elements Zn and Tc is required. Similar to the results shown for Cu and Ga in Sec. III this includes the *ab initio* calculation of vibrational, electronic, and magnetic free-energy contributions. The results in Fig. 6(b) show that the difference between explicitly calculated finite-temperature entropy terms and the screening based on $T = 0$ K energies is 40 K for Zn and 85 K for Tc. The difference in the competition energies at 0 K arises due to the zero point vibrations as compared to the estimates based on 0 K calculations. For both alloying elements, the required corrections for the formation temperature and competition energy are sufficiently small to justify the screening strategy. Furthermore, the analysis in the Supplemental Material demonstrates that the correction from a full decomposition to a partial decomposition is in the case of Zn very similar to that in the Ga case. Hence, the partial decomposition of the the $\text{CeFe}_{11}\text{Ti}$ phase sets in at higher temperatures than 620 K, but remains even at very low temperatures incomplete.

V. IMPACT OF ADDITIONAL PHASES IN Ce-Fe-Ti-X

Comparing the *ab initio* predictions with experiments for a high-throughput screening of phase stabilities reveals that the number of phases considered in the previous section is incomplete. More precisely, we performed SC and RCM experiments to know which additional phases need to be taken into account. The RCM method has proved its value as a high-throughput screening technique for the search of new permanent magnetic phases in complex alloy systems with and without RE elements [56,81] (schematic explanation of the method has been given in Fig. S8). Therefore, we previously used it to benchmark our theoretical findings for phase stabilities in the case of the ternary Ce-Fe-Ti system [36]. We now extended the evaluation to the quaternary Ce-Fe-Ti-X ($X = \text{Cu, Ga, Co and Cr}$) system at two different temperatures ($T = 1123$ K and 1273 K).

For the ternary system [36], we already noticed that the quantitative value of the critical temperature for the 1:12 phase is higher in the RCM experiment than in theory, which might be an effect of the limited diffusion kinetics [82] in the RCM samples. Therefore, we compare in the present work the RCM findings against conventional SC, mostly provided in the Supplemental Material (see Fig. S9). The fact that the observed phases are almost the same gives further confidence in the experimental results.

We start the comparison of the RCM and SC results for Ce-Fe-Ti at 1273 K, from which the phase diagrams, Fig. 7, are obtained. Additionally, the RCM results at 850 °C are also shown for comparison [Fig. 7(a)]. Both phase diagrams consistently indicate the formation of the Fe_2Ti and CeFe_2 Laves phases and the 1:12 phase, confirming our selection of relevant phases in the competition energy model in Eq. (10). In the case of the RCM method, however, the $\text{Th}_2\text{Zn}_{17}$ -type (referred to as 2:17) and/or the $\text{Ce}_3(\text{Fe,Ti})_{29}$ -type (referred to as 3:29) phases are observed, which are missing in SC. The main reason for the observation of the RE-richer compositions (2:17 and 3:29) in the phase diagrams obtained from the RCM studies can be explained as in the following: In the case of RCM, the diffusion is in between the pure elements which leads to different compositional gradients than the SC method, where the chemical composition is strictly restricted. Due to the diffusion pairs between the pure elements the observed gradients in the RCM leads to the formation of RE-lean and RE-rich versions of the possible equilibrium phases. In the case of suction casting, the overall composition of the sample is fixed, which leads to the observation of limited phases in the phase diagram. As the selected composition of the investigated sample lays in the mixed phase region of the phase diagram we observed the 1:12, Fe_2Ti , and CeFe_2 -Laves phases.

The 3:29 phase is stable at high temperatures and is also interesting for room-temperature magnetic applications [84]. However, it was reported in the literature [85] that it is difficult to synthesize the $\text{RE}_3(\text{Fe,Ti})_{29}$ phase ($\text{RE} = \text{Ce, Pr, Nd, and Sm}$) at room temperature, as it is metastable and can only be formed if the equilibrium room-temperature phase has the rhombohedral structure of 2:17. Therefore, we focus on the 2:17 phase in the upcoming considerations, though an integration into a competition formalism similar to Eq. (10)

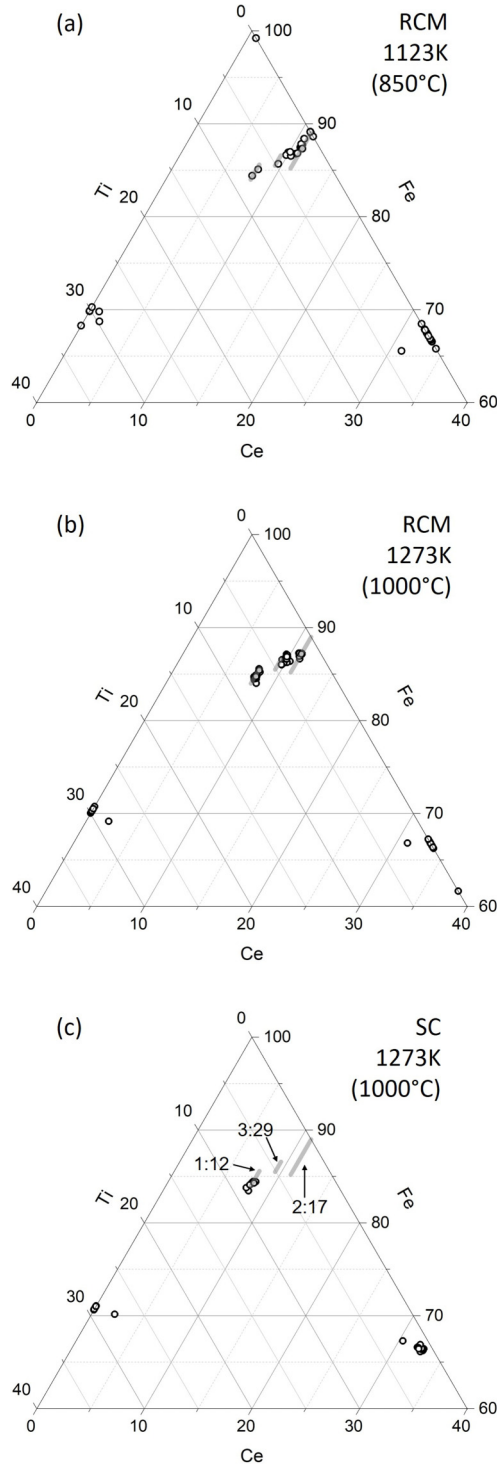


FIG. 7. Fe-rich region of the ternary phase diagram of Ce-Fe-Ti obtained by reactive crucible melting [RCM, (a), (b)] and the suction casting [SC, (c)] at 1123 K and 1273 K. The gray lines represent the Fe contents of the 1:12 (highest), 3:29, and 2:17 phases, respectively. The composition regions for Ti are determined similarly to Margaritan *et al.* [83].

is beyond the scope of this work. In particular, we carefully studied in our *ab initio* approach the stabilization of the 2:17 phase by Ti substitution.

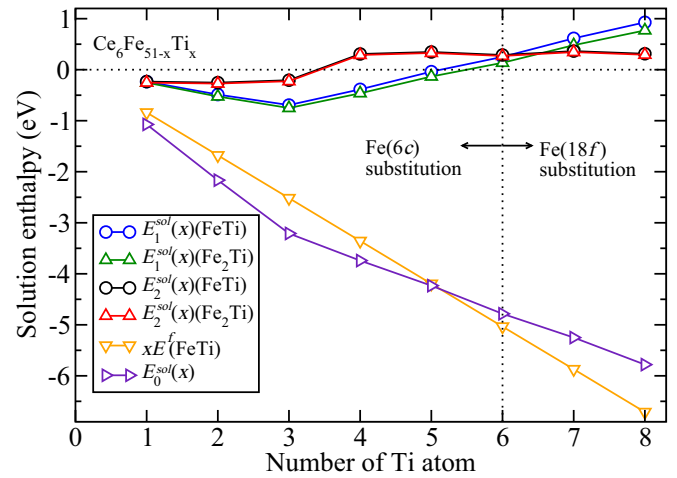


FIG. 8. Calculated Ti solution enthalpies in rhombohedral $\text{Ce}_2\text{Fe}_{17}$ according to the Eqs. (25), (26), and (28). Ti atoms are substituted at energetically favorable 6c sites. Once that site is filled the second energetically favorable 18f site is considered in a $\text{Ce}_6\text{Fe}_{51-x}\text{Ti}_x$ supercell. In all cases, the energetically most favorable configuration is considered. The $xE^f(\text{FeTi})$ line is included for comparison.

The structural parameters of $\text{Ce}_2\text{Fe}_{17}$ are obtained from x-ray diffraction by Buschow *et al.* [86]. The rhombohedral $\text{Ce}_2\text{Fe}_{17}$ has five sublattices, Fe atoms distributed over 6c, 9d, 18f, and 18h sites and Ce atoms occupy the 6c site. To investigate the effect of Ti solubility on the 2:17 phase stability, we start substituting a single Ti atom in a 57 (3 f.u.) atom supercell, corresponding to 1.75 at. % Ti and evaluate the solution enthalpy for all the possible sites. The lowest energy is found for Ti at the 6c site with -1.07 eV. The solution enthalpies for the 9d, 18f, and 18h sites are 14.6 meV/atom, 8.3 meV/atom, and 12.8 meV/atom higher, respectively. The Ce 6c is the energetically least feasible site with 27.2 meV/atom. This strong preference of the 6c site among the Fe sublattices can be due to the large Wigner-Seitz radius compared to other Fe sites [87].

Once the 6c site is found to be energetically favorable, the rest of the 5 Ti atoms are only substituted at this site and the energies are compared in Fig. 8. Since the sixth Ti substitution has slightly positive solution enthalpies, we need to further check its solubility. Once the 6c site is filled, we substitute two more Ti atoms to the second energetically favorable site, namely, 18f. The resulting solution enthalpies are also shown in Fig. 8. We note that for a given Ti concentration, all the possible configurations of 6c and 18f sites are investigated and the energetically most favorable configuration is taken into account. To calculate the solution enthalpies, various kinds of reference alloys are considered. First, the solution enthalpy of a phase can be calculated from unary references

$$E^f(\text{Ce}_6\text{Fe}_{51-x}\text{Ti}_x) = E(\text{Ce}_6\text{Fe}_{51-x}\text{Ti}_x) - 6\mu_{\text{Ce}} - (51-x)\mu_{\text{Fe}} - x\mu_{\text{Ti}} \quad (23)$$

$$= 3E^f(\text{Ce}_2\text{Fe}_{17}) + E_0^{\text{sol}}. \quad (24)$$

In the second equation, the same result is expressed in terms of the formation energy of the unstable 2:17 phase $E^f(\text{Ce}_2\text{Fe}_{17})$.

The correction is provided by the Ti solution enthalpy for the considered phase, for which different formulations can be used. The natural references are also in this case the unary elements

$$E_0^{\text{sol}}(x) = E(\text{Ce}_6\text{Fe}_{51-x}\text{Ti}_x) - 3E^f(\text{Ce}_2\text{Fe}_{17}) + x(\mu_{\text{Fe}} - \mu_{\text{Ti}}). \quad (25)$$

As shown in Fig. 8, E_0^{sol} has a convex negative curvature for the considered number of Ti substitutions. Therefore, taking the unstable positive value of $E^f(\text{Ce}_2\text{Fe}_{17})$ in Eq. (23), all x values result into compositions that are relevant for the discussion of phase stabilities.

There are also different possibilities to incorporate the Ti atom into the microstructure, which are FeTi and Fe₂Ti phases. Those are the thermodynamically stable Fe-Ti alloys, which have negative formation energies compared to unary Fe and Ti and investigated in our previous work [36]. There is a strong chemical driving force for this scenario that is represented by the $xE^f(\text{FeTi})$ line in Fig. 8. In this way, the effective solution enthalpy of the Ti atom in the Ce₂Fe₁₇ phase is given with respect to the chemical potential of Ti in FeTi (or Fe₂Ti):

$$E_1^{\text{sol}}(x) = E(\text{Ce}_6\text{Fe}_{51-x}\text{Ti}_x) - 3E^f(\text{Ce}_2\text{Fe}_{17}) - xE(\text{FeTi}) + 2x\mu_{\text{Fe}} \quad (26)$$

$$= E_0^{\text{sol}}(x) - xE^f(\text{FeTi}). \quad (27)$$

By using this definition, it can be seen in Fig. 8 that the substitution of three Ti atoms into the 57 atom supercell of Ce₂Fe₁₇ (5.26 at. % Ti) yields an energetically global minimum for the system and results in positive enthalpy values beyond five Ti atoms (8.77 at. % Ti).

One can further modify the way of expression by considering FeTi (or Fe₂Ti) and a Ce₂Fe₁₇ structure with lower Ti content as a reference

$$E_2^{\text{sol}}(x) = E(\text{Ce}_6\text{Fe}_{51-x}\text{Ti}_x) - E(\text{Ce}_6\text{Fe}_{51-x+1}\text{Ti}_{x-1}) - E(\text{FeTi}) + 2x\mu_{\text{Fe}}. \quad (28)$$

As shown in Fig. 8, the global minima of the solution enthalpy is obtained for the second Ti atom (3.50 at. %) and yields positive energies beyond third Ti atom. This indicates that a 2:17 structure with three Ti atoms and the formation of FeTi (or Fe₂Ti) is energetically more favorable. The systematic study of solubility energies shows promising agreement with RCM experiments. As seen in the RCM diagram (Fig. 7), the 2:17 phase observed with an off-stoichiometric composition of two to three at. % Ti corresponds to 1.5 atoms in the 57 atom supercell, which is slightly lower than the E_2^{sol} formulation results. A similar strategy was applied to the 1:12 phase in our previous work [36] and Ti solubility was found as 7.7 at.%. This prediction compares also well against the experimental data given a Ti solubility in the 1:12 phase at ~9 at.% (see Fig. 7). In this way, the higher Ti solubility of the 1:12 phase compared to the 2:17 one is also proven.

The RCM studies on Ce-Fe-Ti alloys that contain different alloying elements are for the two different temperatures 1123 K and 1273 K given in Fig. 9. While the measurement

points are indicated by circles, the gray lines represent the composition regions of the 1:12, 2:17, and 3:29 phases as extracted from the work of Margarian *et al.* [83], similar to Fig. 7. The axes of the quaternary phase diagrams corresponds to Ce, Ti, and the summation of the Fe and the added element X. To be able to present a quaternary phase stability on a ternary phase diagram, we use different color codes for the composition of the added fourth element. The corresponding value of the compositions of X is given in the color scale.

The observed phase distribution in the RCM phase diagram of the Ce-Fe-Ti-Cu system is different from that of the ternary Ce-Fe-Ti system [see Figs. 7(a) and 7(b)]. The Cu addition suppresses the formation of the 1:12-type phase at 1123 K and assists the formation of the binary B2-FeTi as well as Ce-Cu binary phases (not shown in the diagram, full-scale phase diagrams are given in the Supplemental Material, see Fig. S9). As revealed by RCM in Fig. 9, the Cu solubilities in the 1:12 and the Fe₂Ti phases are nearly zero and is very limited in CeFe₂, which is consistent with our formation enthalpy calculations given in Fig. 3.

Therefore, instead of substituting any of the considered competing phases, it is energetically more favorable for the excess amount of Cu to form new Ce-Cu binaries. The formation energies of the possible Ce-Cu compounds were investigated computationally, shown in Fig. 10 (top). It can be seen that the orthorhombic CeCu₂ phase (space group *Imma*) has the lowest formation energy. Apparently, the fact that we did not consider the formation of Ce-Cu binaries and the B2-FeTi phase in our competition energy formalism drives an artificially high amount of Cu into the CeFe₂ phase (as indicated in Fig. 4) and destabilizes the 1:12 phase more than observed in experiment (see Fig. 1).

The observed phase distribution after adding Ga is showing the formation of Ce-Ga binary phases more clearly, with composition ranges varying from Ce_{68.0}Ga_{32.0} to Ce_{59.6}Fe_{7.7}Ti_{1.8}Ga_{30.9}. Again, there are no indications in the RCM measurements that a 1:12 phase is stable at 1123 K. It is only observed once the temperature increases to 1273 K. In comparison to Fig. 10, this can be interpreted such that Ga substitution destabilizes the desired hard magnetic phase, seemingly in conflict with our theoretical results (see Fig. 1).

However, also in the case of Ga, the RCM as well as the SC studies indicate the formation of Ce-(Ga,Fe) RE-rich phases such as CeGa. The investigations of formation energies given in Fig. 10 indicates substantially larger absolute values than in the case of Cu. The hexagonal CeGa₂ phase (space group *P6/mmm*) has the lowest formation energy. Therefore, Ga does not tend to substitute one of the considered competing phases but forms new binaries. Furthermore, the SC results indicate a substantial solubility of the Ga in both Laves phases with more complex compositions like (Fe,Ga,Ce)₂Ti and Ce(Fe,Ti,Ga)₂. Therefore, the observed differences might be explained by the fact that the theoretical predictions were only done for ternary and not for quaternary compositions of the Laves phases. The SC results for Cu additions do not show such a Cu substitution in the Ce(Fe,Cu)₂ Laves phase.

In the case of Co and Cr substituted quaternary RCM diagrams, the observed phases are similar to the Ce-Fe-Ti ternary and an increasing temperature has no significant impact on the stability of phases. For both substitutions, the 1:12

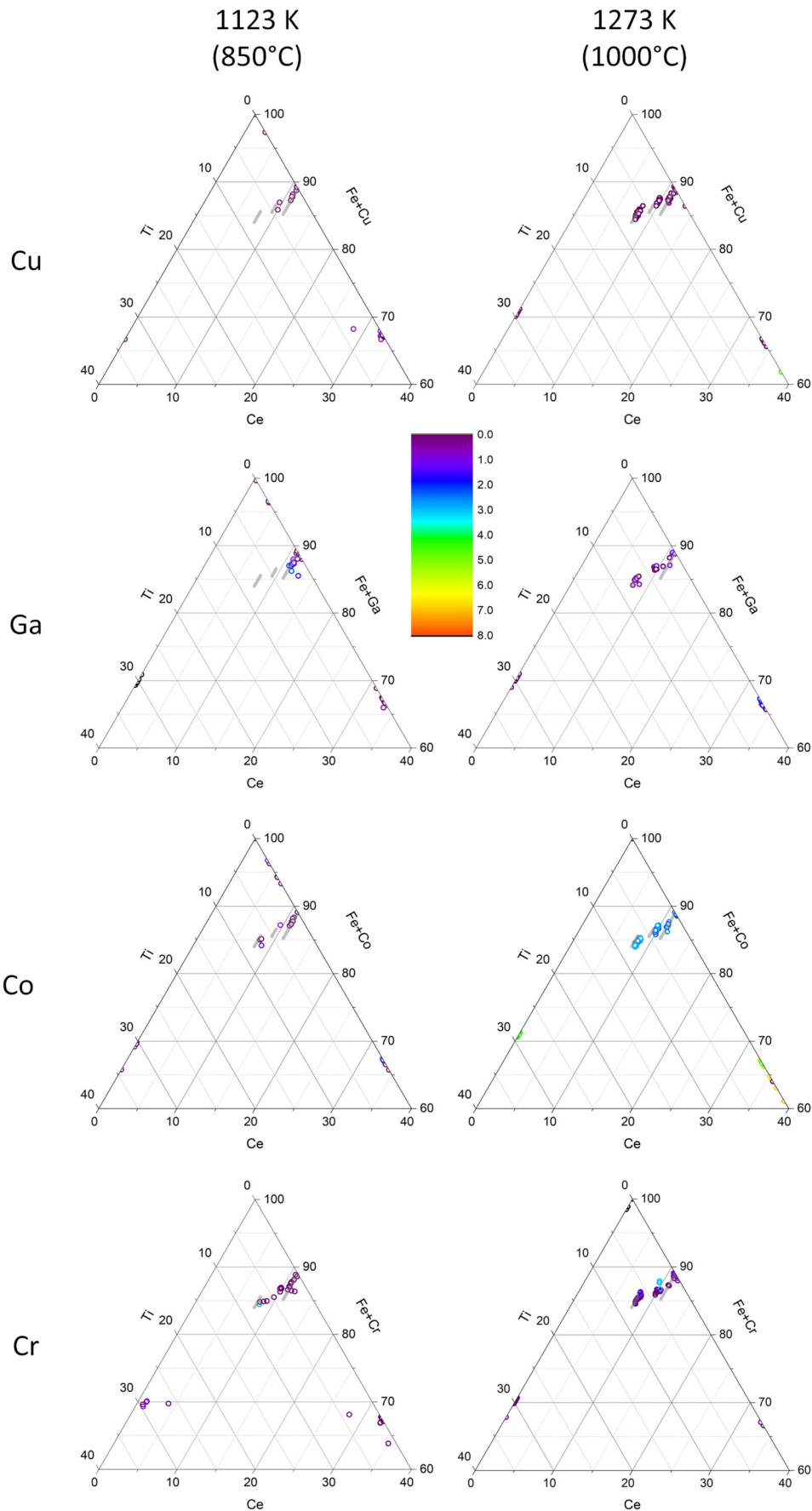


FIG. 9. RCM diagrams of the Ce-Fe-Ti-X ($X = \text{Cu, Ga, Co, and Cr}$) quaternary systems processed at 1123 K and 1273 K. Each symbol indicates a measurement point obtained from the reactive crucible. The chemical composition of the X element is given by the color scales up to 8 at.%. The values above 8 at.% are indicated by the black color in the graphs. The gray lines represent the composition regions of the 1:12, 3:29, and 2:17 phases as described in the caption of Fig. 7. The diagrams show Fe-rich regions, for the full scale RCM phase diagrams see Fig. S10.

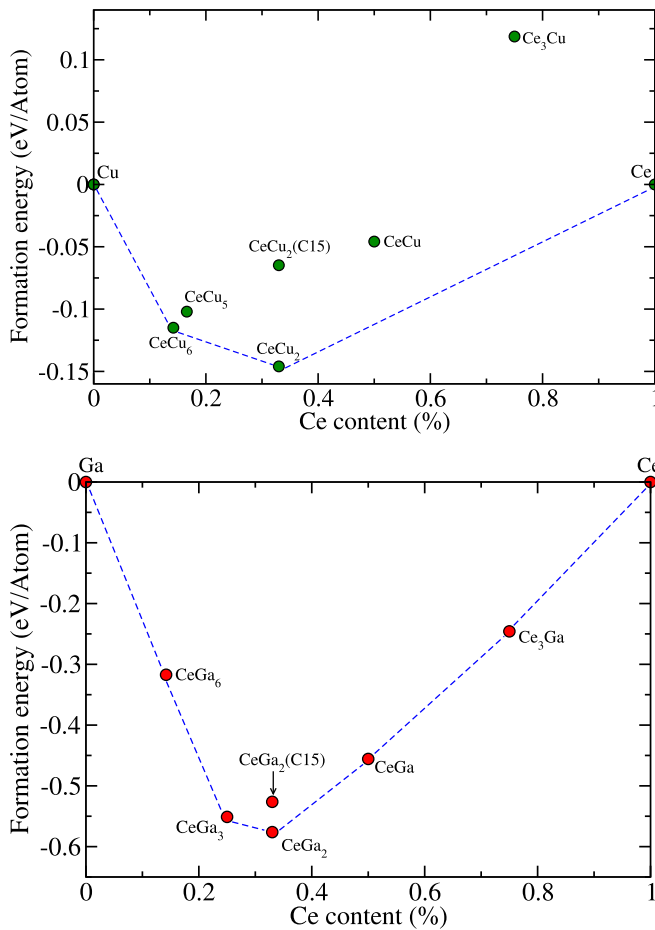


FIG. 10. Calculated formation energies for Ce-Cu (top) and Ce-Ga binaries (bottom).

phase exists and this can be interpreted such that Co and Cr substitutions have no hazardous effect on the stability of the desired phase. This is also predicted in our screening calculations, where the formation temperature of the 1:12 phase is calculated to be 744 and 905 K for Co and Cr substitutions, respectively. There are remarkable differences for the distribution of Co and Cr over the different phases. According to the theoretical prediction of Fig. 4, Cr is not expected in any of the Laves phases. Instead a Cr incorporation into α -Fe is expected due to the very low formation enthalpy shown in Fig. 3. In contrast to this, a substantial Co content is expected in the CeFe₂ phase as shown in Fig. 4. These predictions are confirmed by the RCM results.

For the 1:12 phase, the negative enthalpies for the substitution of Co and Cr provided in Fig. 3 are consistent with the observation of a noticeable atomic fraction of these elements in the RCM measurements. For example, the Cr content in the 1:12 is about 3 at.%, substantially larger than Cr content of 1 at.% in the Fe₂Ti phase, for example. It is interesting to note a clear temperature dependence of the substitutional concentration in the 1:12 phase. To explain this theoretically, the full formalism of partial decomposition would need to be applied to Co and Cr. By comparing the solution enthalpies in Fig. 3, we would expect that Cr behaves similarly to Ga, for which the substitutional content in the 1:12 should decrease

with temperature. The behavior of Co should be closer to that of Cu, for which we expect an enrichment of the solute in the competing phases with increasing temperature. The incomplete matching of theory and experiment in this case indicates that the RCM measurements are not representing thermodynamic equilibrium.

VI. DISCUSSION AND CONCLUSION

By using a combination of *ab initio* calculations and experimental methods, we analyzed the impact of substitutional alloying elements on the thermodynamic stability of structural phases in the Ce-Fe-Ti-X system. Our free-energy calculations contain all relevant entropy contributions, of which the magnetic entropy turns out to be particularly important. The calculations reveal that the critical temperature for the formation of the hard-magnetic phases CeFe₁₁Ti in the ternary Ce-Fe-Ti system is 710 K. Below this temperature, it decomposes into the energetically more favorable competing Laves phases CeFe₂ and Fe₂Ti as well as pure Fe.

To reduce this temperature of formation, alloy substitutions of up to 3 at.% are applied. The examples of Cu and Ga are used to provide some fundamental methodological insights. One of them is the concept of a partial decomposition, which considers the enrichment of the added solutes in phases that would, at the considered temperature, not be stable in a full decomposition. In the case of Cu, this effect suppresses the formation of phase pure CeFe₁₁Ti even at temperatures well above 1500 K, whereas in the case of Ga this ensures the presence of a small phase fraction of CeFe₁₁Ti even below the critical temperature.

The other conclusion derived from study on Cu and Ga is the dominant impact of 0 K formation enthalpies on the solute-enhanced phase stability compared to finite-temperature entropy terms. Based on this insight, a screening approach, considering the substitution of all 3d and 4d elements, is performed in which the energies of formation at 0 K are taken as the most important selection criterion. For most of the transition metals we observe a preference of substituting Fe sites in CeFe₁₁Ti and the Laves phases. Only a few transition metals were not considered further because their preference of the Ce or Ti sites additionally complicates the determination of a consistent set of chemical potentials. We show that substituted elements with more than a half-filled 3d-shell (except Cu) or with less than a half-filled 4d-shell mainly reduce the formation temperature of the 1:12 phase. According to these thermodynamic considerations, especially Zn and Tc turn out to be promising substitution candidates. Therefore, more detailed finite temperature *ab initio* evaluations of the free energies were performed for these elements. The difference between the approximate determination of the critical temperature for the formation of the CeFe₁₁Ti based on 0 K energies and a fully temperature-dependent determination of free energies is within the error bar of the other approximations. This demonstrates the robustness and efficiency of our screening approach.

In addition to this, the partitioning of the considered substitutional elements among the competing phases is also predicted correctly for many cases. Nevertheless, the comparison with experimental data from reactive crucible melting and

suction casting reveals that the number of competing phases that entered our theoretical model is insufficient for many of the substitutions by transition metals. Instead, a number of additional phases are observed in these experiments, which increases the complexity of the thermodynamic equilibrium. An extension of the thermodynamic phase stability analysis to the full quaternary phase diagram of Ce-Fe-Ti-X, including the impact of solubility ranges in the relevant phases, needs to be subject to further studies.

ACKNOWLEDGMENTS

Our project on rare-earth-based alloys for hard-magnetic applications: temperature and pressure-dependent phase stabilities (RE-MAP) is supported by Deutsche Forschungsgemeinschaft (DFG Project No. 316912154). The partial finance by Bosch-Forschungsförderung for this work is acknowledged. We are also grateful to Silke Biermann, Leonid V. Pourovski, and Anna Galler for fruitful discussions.

-
- [1] L. Kahle, A. Marcolongo, and N. Marzari, *Energy Environ. Sci.* **13**, 928 (2020).
- [2] D. Dahliah, G. Brunin, J. George, V. A. Ha, and G. Rignanese, G. Hautier, *Energy Environ. Sci.* **14**, 5057 (2021).
- [3] O. Gutfleisch, M. Willard, E. Brück, C. H. Chen, S. G. Sankar, and J. P. Liu, *Adv. Mater.* **23**, 821 (2011).
- [4] J. J. Croat, J. F. Herbst, R. W. Lee, and F. E. Pinkerton, *J. Appl. Phys.* **55**, 2078 (1984).
- [5] M. Sagawa, S. Fujimura, N. Togawa, H. Yamamoto, and Y. Matsuura, *J. Appl. Phys.* **55**, 2083 (1984).
- [6] D. Bauer, D. Diamond, J. Li, D. Sandalow, P. Telleen, and B. Wanner, U.S. Department of Energy, Tech. Rep. (U.S. Department of Energy, 2011).
- [7] M. Pellegrini, Report on Critical Raw Materials for the Eu Critical Raw Materials Profiles, Tech. Rep. (2014).
- [8] N. Drebov, A. Martinez-Limia, L. Kunz, A. Gola, T. Shigematsu, T. Eckl, P. Gumbsch, and C. Elsässer, *New J. Phys.* **15**, 125023 (2013).
- [9] W. Körner, G. Krugel, and C. Elsässer, *Sci. Rep.* **6**, 24686 (2016).
- [10] H. I. Sözen and T. Klüner, *J. Magn. Magn. Mater.* **559**, 169529 (2022).
- [11] K. P. Skokov and O. Gutfleisch, *Scr. Mater.* **154**, 289 (2018).
- [12] I. Poenaru, A. Lixandru, S. Riegg, B. Fayyazi, A. Taubel, K. Güth, R. Gauß, and O. Gutfleisch, *J. Magn. Magn. Mater.* **478**, 198 (2019).
- [13] S. Massari and M. Ruberti, *Resources Policy* **38**, 36 (2013).
- [14] G. Tyler, *Plant and Soil* **267**, 191 (2004).
- [15] Y. Hirayama, Y. Takahashi, S. Hirosawa, and K. Hono, *Scr. Mater.* **95**, 70 (2015).
- [16] Y. Hirayama, Y. K. Takahashi, S. Hirosawa, and K. Hono, *Scr. Mater.* **138**, 62 (2017).
- [17] F. Maccari, L. Schäfer, I. Radulov, L. Diop, S. Ener, E. Bruder, K. Skokov, and O. Gutfleisch, *Acta Mater.* **180**, 15 (2019).
- [18] S. Ener, K. P. Skokov, D. Palanisamy, T. Devillers, J. Fischbacher, G. Gomez, F. Maccari, L. Schäfer, L. V. B. Diop, I. Radulov, B. Gault, G. Hrkac, N. M. Dempsey, T. Schrefl, D. Raabe, and O. Gutfleisch, *Acta Mater.* **214**, 116968 (2021).
- [19] A. Alam, M. Khan, R. W. McCallum, and D. D. Johnson, *Appl. Phys. Lett.* **102**, 042402 (2013).
- [20] O. Isnard, *J. Alloy. Compd.* **356-357**, 17 (2003).
- [21] M. Akayama, H. Fujii, K. Yamamoto, and K. Tatami, *J. Magn. Magn. Mater.* **130**, 99 (1994).
- [22] D. Fruchart, F. Vaillant, A. Yaouanc, J. M. D. Coey, R. Fruchart, P. L'heritier, T. Riesterer, J. Osterwalder, and L. Schlapbach, *J. Less-Common Met.* **130**, 97 (1987).
- [23] T. W. Capehart, R. K. Mishra, G. P. Meisner, C. D. Fuerst, and J. F. Herbst, *Appl. Phys. Lett.* **63**, 3642 (1993).
- [24] P. Dalmas de Reotier, D. Fruchart, L. Pontonnier, F. Vaillant, P. Wolfers, A. Yaouanc, J. M. D. Coey, R. Fruchart, and P. L'heritier, *J. Less-Common Met.* **129**, 133 (1987).
- [25] J. F. Herbst, M. S. Meyer, and F. E. Pinkerton, *J. Appl. Phys.* **111**, 07A718 (2012).
- [26] C. J. Yan, S. Guo, R. J. Chen, D. Lee, and A. R. Yan, *Chin. Phys. B* **23**, 107501 (2014).
- [27] M. Xing, J. Han, Z. Lin, F. Wan, C. Li, S. Liu, C. Wang, J. Yang, and Y. Yang, *J. Magn. Magn. Mater.* **331**, 140 (2013).
- [28] E. Niu, Z. A. Chen, G. A. Chen, Y. G. Zhao, J. Zhang, X. L. Rao, B. P. Hu, and Z. X. Wang, *J. Appl. Phys.* **115**, 113912 (2014).
- [29] M. Zhang, Y. Liu, Z. Li, L. Peng, B. Shen, and F. Hu, *J. Alloys Compd.* **688**, 1053 (2016).
- [30] C. Yan, S. Guo, R. Chen, D. Lee, and A. Yan, *IEEE Trans. Magn.* **50**, 2104604 (2014).
- [31] Z. Chen, Y. K. Lim, and D. Brown, *IEEE Trans. Magn.* **51**, 2102104 (2015).
- [32] Q. Y. Zhou, Z. Liu, S. Guo, A. R. Yan, and D. Lee, *IEEE Trans. Magn.* **51**, 2104304 (2015).
- [33] X. Chen, Y. G. Chen, Y. B. Tang, and D. Q. Xiao, *Rare Metals* **35**, 691 (2016).
- [34] M. Zhang, Z. Li, B. Shen, F. Hu, and J. Sun, *J. Alloys Compd.* **651**, 144 (2015).
- [35] L. Paolasini, P. Dervenagas, P. Vulliet, J. P. Sanchez, G. H. Lander, A. Hiess, A. Panchula, and P. C. Canfield, *Phys. Rev. B* **58**, 12117 (1998).
- [36] H. I. Sözen, S. Ener, F. Maccari, K. P. Skokov, O. Gutfleisch, F. Körmann, J. Neugebauer, and T. Hickel, *Phys. Rev. Mater.* **3**, 084407 (2019).
- [37] W. F. Li, T. Ohkubo, T. Akiya, H. Kato, and K. Hono, *J. Mater. Res.* **24**, 413 (2009).
- [38] P. Yi, M. Lin, R. Chen, D. Lee, and A. Yan, *J. Alloys Compd.* **491**, 605 (2010).
- [39] J. Ni, T. Ma, and M. Yan, *J. Magn. Magn. Mater.* **323**, 2549 (2011).
- [40] G. Kresse and J. Hafner, *Phys. Rev. B* **47**, 558 (1993).
- [41] G. Kresse and J. Furthmüller, *Phys. Rev. B* **54**, 11169 (1996).
- [42] P. E. Blöchl, *Phys. Rev. B* **50**, 17953 (1994).
- [43] J. P. Perdew, K. Burke, and M. Ernzerhof, *Phys. Rev. Lett.* **77**, 3865 (1996).
- [44] See Supplemental Material at <http://link.aps.org/supplemental/10.1103/PhysRevMaterials.7.014410> which contains additional references [1,2] on computational details and the treatment of *f*-electrons.

- [45] T. Hickel, B. Grabowski, F. Körmann, and J. Neugebauer, *J. Phys.: Condens. Matter* **24**, 053202 (2012).
- [46] D. C. Wallace, *Thermodynamics of Crystals* (Dover, New York, 1998).
- [47] N. D. Mermin, *Phys. Rev.* **137**, A1441 (1965).
- [48] H. J. Monkhorst and J. D. Pack, *Phys. Rev. B* **13**, 5188 (1976).
- [49] K. Parlinski, Z. Q. Li, and Y. Kawazoe, *Phys. Rev. Lett.* **78**, 4063 (1997).
- [50] B. Grabowski, T. Hickel, and J. Neugebauer, *Phys. Rev. B* **76**, 024309 (2007).
- [51] G. Inden, in *Proceedings of CALPHAD V* (Max Planck Institute Eisenforschung, Düsseldorf, 1976), pp. 1–13.
- [52] M. Hillert and M. Jarl, *Calphad* **2**, 227 (1978).
- [53] Q. Chen and B. Sundman, *J. Phase Equilib.* **22**, 631 (2001).
- [54] W. Xiong, Q. Chen, P. A. Korzhavyi, and M. Selleby, *CALPHAD* **39**, 11 (2012).
- [55] H. I. Sözen, T. Hickel, and J. Neugebauer, *CALPHAD* **68**, 101731 (2020).
- [56] S. Ener, J. Kroder, K. P. Skokov, and O. Gutfleisch, *J. Alloys Compd.* **683**, 198 (2016).
- [57] B. Fayyazi, K. P. Skokov, T. Faske, D. Y. Karpenkov, W. Donner, and O. Gutfleisch, *Acta Mater.* **141**, 434 (2017).
- [58] D. Goll, R. Loef, D. Hofs, and G. Schneider, *Scr. Mater.* **146**, 355 (2018).
- [59] H. I. Sözen, E. Mendive-Tapia, T. Hickel, and J. Neugebauer, *Phys. Rev. Mater.* **6**, 023603 (2022).
- [60] N. W. Ashcroft and N. D. Mermin, *Solid State Physics* (Saunders College, Philadelphia, 1976).
- [61] X. B. Liu and Z. Altounian, *IEEE Trans. Magn.* **48**, 3144 (2012).
- [62] K. V. Rama Rao, G. Markandeyulu, K. G. Suresh, V. R. Shah, U. V. Varadaraju, M. Venkatesan, M. Q. Huang, K. Sirisha, M. E. Mchenry, and V. G. Harris, *Bull. Mater. Sci.* **22**, 509 (1999).
- [63] E. Burzo, A. Chelkowski, and H. R. Kirchmayr, *Compounds Between Rare Earth Elements and 3d, 4d or 5d Elements*, New sSeries ed., edited by H. Wijn, (Springer-Verlag, Berlin, 1990).
- [64] F. H. Spedding, A. H. Daane, and K. W. Herrmann, *Acta Crystallogr.* **9**, 559 (1956).
- [65] S. Allard, *Metals, Thermal and Mechanical Data: International Tables of Selected Constants*, Vol. 16, (Pergamon, Oxford, 1969).
- [66] D. I. Bolef, R. E. Smith, and J. G. Miller, *Phys. Rev. B* **3**, 4100 (1971).
- [67] J. L. Murray, *J. Phase Equilib.* **19**, 367 (1998).
- [68] C. S. Barrett, *Structure of Metals: Crystallographic Methods, Principles, and Data*, 3rd ed. (Permagon, New York, 1980).
- [69] W. B. Pearson, *A Handbook of Lattice Spacings and Structures of Metals and Alloys*, 1st ed., edited by G. V. Raynor (Pergamon, New York, 1958).
- [70] D. E. Gray, *American Institute of Physics Handbook*, 3rd ed., (McGraw-Hill, New York, 1970).
- [71] R. W. Lynch and H. G. Drickamer, *J. Phys. Chem. Solids* **26**, 63 (1965).
- [72] S. K. Sinha, T. O. Brun, L. D. Muhlestein, and J. Sakurai, *Phys. Rev. B* **1**, 2430 (1970).
- [73] E. S. Fisher and C. J. Renken, *Phys. Rev.* **135**, A482 (1964).
- [74] J. Trivisonno, S. Vatanayon, M. Wilt, J. Washick, and R. Reifenberger, *J. Low Temp. Phys.* **12**, 153 (1973).
- [75] G. Simons and H. Wang, *Single Crystal Elastic Constants and Calculated Aggregate Properties: A Handbook* (M.I.T. Press, Cambridge, MA, 1971).
- [76] J. Donohue, *The Structures of the Elements*, edited by R. Krieger (Krieger, Malabar FL, 1982).
- [77] R. L. Clendenen and H. G. Drickamer, *J. Phys. Chem. Solids* **25**, 865 (1964).
- [78] H. P. Singh, *Acta Cryst. A* **24**, 469 (1968).
- [79] V. Hansen, *Constitution of Binary Alloys* (McGraw-Hill, New York, 1958).
- [80] J. Xu, Phase formation and transformation in the R-Fe-T systems: (R = Nd, Gd, Tb, Dy, Er, Ho, Tm and Lu, T = Si, Ti and Zr), Ph.D. thesis, University of Wollongong, 1996.
- [81] F. Gross, Search for new permanent magnetic phases by the reaction crucible analysis and development of new high through put methods, Ph.D. thesis, University of Birmingham, 2004.
- [82] H. I. Sözen, *Comput. Mater. Sci.* **214**, 111712 (2022).
- [83] A. Margarian, J. B. Dunlop, R. K. Day, and W. Kalceff, *J. Appl. Phys.* **76**, 6153 (1994).
- [84] K. Sirisha, M. Q. Huang, M. E. Mchenry, Q. Chen, and M. B. Ma, *J. Appl. Phys.* **87**, 5275 (2000).
- [85] C. D. Fuerst, F. E. Pinkerton, and J. F. Herbst, *J. Appl. Phys.* **76**, 6144 (1994).
- [86] K. H. J. Buschow and J. S. van Wieringen, *Phys. Status Solidi (b)* **42**, 231 (1970).
- [87] D. Hautot, G. J. Long, F. Grandjean, and O. Isnard, *Phys. Rev. B* **62**, 11731 (2000).